Institute of Photogrammetry and Geoinformatics

Flood Detection with a Deep Learning Approach Using Optical and SAR Satellite Data

Master thesis

Degree Program: Geodesy and Geoinformatics

Author: Sara El Amrani Abou El Assad
First Examiner: Dr. Sanaz Vajedian
Second Examiner: Prof. Dr.-Ing. Christian Heipke

Start Date: 30.05.2019
End Date: 30.11.2019

1 Undertaking

I declare that the work presented in this dissertation report entitled "Flood Detection with a Deep Learning Approach Using Optical and SAR Satellite Data", submitted to IPI institute, Leibniz University Hannover, for the award of the degree, Master of Science in Geodesy and Geoinformatics is my original work. I have not plagiarized or submitted the same work for the award of any other degree.

Hannover, 29.11.2019

(Sara El Amrani Abouelassad)

2 Abstract

This study presents an approach to automatically detect flood regions using satellite data. This proposed method is applicable for urban and bare soil areas. For this purpose, data from two sensors with different modalities are used. The first dataset is radar data acquired from Sentinel-l A/B satellites that provide complex data in the two co- and cross polarizations (VV and VH). The second dataset is optical data acquired from Sentinel-2 A/B satellites that provide multispectral data of 13 bands ranging from visible to short infra-red parts of the electromagnetic spectrum. The use of radar data is advantageous given that it is independent of any kind of weather conditions unlike optical data that are not able to acquire data in cloudy regions. Moreover, radar data can be useful for flood mapping because water bodies appear as dark areas due to the backscattering effect of water. On the other hand, water surface reacts differently in terms of reflection and absorption in different wavelengths from visible to shortwave infra-red. Therefore, multispectral optical data are able to recognize water bodies.

Detecting floods in a fast and precise way is crucial as it helps in improving crisis management and consequently reducing damages of the natural disaster phenomenon. Deep neural networks are demonstrating improvement in their ability to handle big data to implement variety of tasks such as object detection, change detection, and object classification. In this study, we use supervised deep learning network, that is considered as one of the latest trending methods in remote sensing, to map flood areas using radar and optical satellite data. Specifically, we use Siamese neural networks to detect the water bodies resulting from flood events by applying simultaneously semantic segmentation over pre- and post-event images to produce feature maps. The difference between the feature maps derived from pre- and post-event images reveals the flood region. The supervised proposed approach is trained using reference data that was created in this study using the optical and radar data of two different flood regions in Iran. Part of the data was kept for testing, and the results show that the developed methods could detect flood areas with an accuracy around 94.67% using optical data and an accuracy of around 81%.

Contents

1 Undertaking **i**

2 Abstract **ii**

3 Introduction **1**

3.1 Problem and Motivation 1

3.2 Related Work 2

4 Theoretical Background **3**

4.1 Remote Sensing 3

4.1.1 Radar Remote Sensing 4

4.1.2 Optical Remote sensing 6

4.2 Deep Learning 9

4.2.1 Convolutional Neural Networks 11

4.2.2 U-net 13

4.2.3 Siamese Neural Networks 14

4.3 Flood Mapping 15

4.4 Conclusion 17

5 Proposed Flood Detection Model **17**

5.1 U-net 17

5.2 Networks 18

6 Experimental Settings **19**

6.1 Data Acquisition and Pre-processing 19

6.1.1 Study Area 20

6.1.2 Data Collection 21
6.1.3 Data Labeling 26
6.1.4 Data Normalization 28
6.1.5 Data Augmentation 29
6.2 Network Structure implementation 29
6.3 Evaluation Metrics 29

7 Experimental Results **30**
7.1 Training Algorithm Parameters 31
7.2 Flood Mapping Results 33
7.3 Discussion 36

8 Conclusion **37**

List of Figures

1 Backscattering of dry, wet, and flooded soils 5

2 Double bounce effect 6

3 Imaging of a building by and optical sensor 8

4 A single node 9

5 A U-net architecture 14

6 Reflectance of clear and turbid water with respect to the wavelengths of band 3 and band8 16

7 Overall network 19

8 An aerial view of flooding in Khuzestan province, Iran, April 5, 2019 . . 21

9 Aq-Qala optical data. (Left: R, NIR, SWIR composite of 11.03.2019. Right: R, NIR, SWIR composite of 05.04.2019) 23

10 Ahwaz optical data. (Left: R, NIR, SWIR composite of 22.03.2019. Right: R, NIR, SWIR composite of 26.04.2019) 24

11 Aq-Qala SAR data. (Left: coherence, intensity VH, intensity VV composite of 11.03.2019. Right: coherence, intensity VH, intensity VV composite of 04.04.2019) 26

12 Final flood mask of Aq-Qala region 27

13 Final flood mask of Ahwaz region 28

14 Optical data based network training and validating accuracies and losses (learning) curves 32

15 SAR data based network training and validating accuracies and losses (learning) curves 33

16 Flood detection results. 34

17 Flood detection results 34

18 Flood detection results 34

19 Flood detection results 35
20 Flood detection results 35
21 Flood detection results 35
22 Flood detection results 36

List of Tables

1 Some of Sentinel 1 characteristics 5
2 Some of Sentinel 2 characteristics 7
3 Sentinel 2 Bands Wavelengths 7
4 Sentinel 2 Bands Wavelengths 22
5 The confusion matrix 29
6 Evaluation results 33

3 Introduction

3.1 Problem and Motivation

The recent years have seen an unpreceded soar of floods around the world. According to [13], inundations have increased in Central Europe by a factor of two since 1980. These floods cause massive economic damages not only to governments, but also individuals and private institutions like insurance companies. For this reason, concerned entities encourage research and development set ups to find new methods to better serve the community and those entities themselves to improve services provided when this kind of phenomena occurs for better crisis response and mitigation. Over recent years, the accessibility of satellite remote sensing enabled the researchers to use the tool in monitoring natural disasters like hydrological disasters and earthquakes. The free access to these products supported users of different background to further extend their investigations with these huge amounts of data. Currently, satellite data can be considered as an effective tool to estimate disaster damages and enhance catastrophe risks because of their sensors' diverse modalities, and their huge volume with various space, time, and spectral resolutions. This data availability allowed the creation of serves that serve for the development of automated or semi-automated methods that serves quick flood mappings. Theses methods have some uncertainties since they are not checked and are rapidly produced. More accurate flood mapping methods are used in case of emergencies like the use of un-manned aerial vehicles photos or field surveys. Nonetheless, techniques are time consuming, costly, and sometimes even not possible to make in bad weather conditions on time. Consequently, new procedures were introduced in remote sensing to raise the current challenges. Neural networks became the new trend in remote sensing because of their success in many computer vision tasks. The contributions of this thesis are the following:

- Studying and highlighting the problems encountered in flood mapping using Synthetic Aperature Radar (SAR) and optical imagery acquired over urban and non-urban areas
- Two end-to-end trainable neural networks for flood detection are proposed using optical and SAR satellite data respectively. The proposed methods also attempt

to map only water bodies resulting from a flood event and not permanent water surfaces.

- We demonstrate the performance of neural networks to detect floods in data acquired from Sentinel 1 and Sentinel 2 missions over Aq-Qala and Ahwaz cities and surrounding suburbs in Iran

The remining of the paper is organized as follows: Chapter II discusses related experiments and work related to change detection and semantic segmentation. Chapter III describes the preprocessing steps of data and the design and structure of the networks used. Chapter IV details the process of the experiment and analyses the results. Finally, chapter V gives a conclusion about the work done.

3.2 Related Work

Flood mapping is a challenging task using traditional methods due to the lack of flood data during floods. Airborne flights have work limitations because of bad weather conditions that follow habitually a flood event. More importantly, it is usually very expensive to produce a flood map within a period of time that is effectively short. Hence, the need to build a method that is reliable and cost effective is the motivation behind this work. The potential market for this solution includes public environmental management agencies, governmental authorities, and insurance companies. Flood mapping is one of the applications where satellite data can be valuable and it will further help in risk management, damage assessment and providing more information to rescuers during flooding. Specifically, optical and SAR satellite data can be used to detect and map floods.

SAR data is useful because measurements are taken regardless of weather conditions and lightening conditions. The sensors of these products are active sensors which use their own energy to send signals to make observations over a space.

Pixel-wise classification methods include rule-based methods, which heavily focuses on finding threshold values to differentiate between water pixels and non-water pixels. Approaches using water indices [17, 6] are rule-based methods using algebra of bands. The efficiency of the aforesaid methods depends on the identification of an ideal thresh-

old. Factors to be considered to find the threshold are spatial resolution of the satellite image, presence of shadow, and the ground area. The last factor in particular requires the calibration of threshold values if different mapped are changes, and limits the generalization of the method. The authors in [] presented several semi-automatic and manual methods to map inundations, by exploiting free satellite multispectral and SAR data.

Because of the success encountered in various research areas, remote sensing is similarly starting to use DNNs as a methodology for many of its applications. However, remote sensing data presents some new challenges for deep learning. For example, in this paper, the datasets used are from optical and SAR sensors and hence, multimodal.

4 Theoretical Background

4.1 Remote Sensing

The use of earth observation data from space can be very useful as it provides valuable and timely information when investigating emergencies such as floods. Another advantage of satellite observation is the ability to acquire large area data even from hard-to-reach regions or during natural disasters like floods. Optical and SAR sensor modalities are under focus of this study.

This section will further give details about SAR and optical data acquired by Sentinel 1 and Sentinel 2 respectively. The datasets used in this thesis are derived from processed image products from the latter satellite missions and they can be described by the following characteristics:

- Space-borne due to the nature of the used sensors
- Multimodal because of the different sensor modalities
- Flood-expansion due to the use of before and after flood data
- Good resolution due to the volume of spatial details available

It is important to understand how a flooded and non-flooded area is imaged. It is a crucial step that enables deciding on the pre-processing steps, labeling to get the ground

truth data, and methodology selection for flood mapping.

4.1.1 Radar Remote Sensing

Sentinel 1 is the first mission of the Copernicus Program satellite constellation by the European Space Agency (ESA), launched in April 2014. The mission consists of two satellites S1A and S1B sharing the same orbital plane [2]. Sentinel 1 satellites are active satellites and they use microwaves in the C-Band to capture topographic information of the earth surface. Table 1 gives basic information about the satellites. Sentinel 1 has 4 imaging modes with varying resolutions:

- StripMap (SM)
  The ground swath is illuminated with a continuous sequence of pulses while the antenna beam is pointed to a fixed angle in azimuth and an approximately fixed off-nadir angle.
- Interferometric Wide (IW)
  It is the main acquisition mode over land. Three ground sub-swaths are captured using Terrain Observation with Progressive Scans SAR (TOPSAR). IW can be used for interferometry.
- Extra Wide (EW)
  Five sub-swaths are captured using the TOPSAR technique.
- Wave (WV)
  Several vignettes are acquired exclusively in either VV or HH polarization, and each vignette processed as a separate image.

Sentinel 1 satellite sensors measure the radar strength of the returned signal and the time it takes for a round trip of the signal to get the range location and brightness (or amplitude) of the pixels. One of the major reasons why SAR data is used in flood detection is due to the ability of microwave instruments of cloud-penetrating and day-and-night operational features. Another valuable advantage of SAR data is microwave backscattering. The backscattering coefficient is the square of the amplitude of the complex signal, and it is affected by surface roughness. Water filled areas are

Table 1: Some of Sentinel 1 characteristics

Sentinel 1	
Resolution	5x5 m SM mode 5x20 m IW mode and WV mode 25x100 m EW mode
Orbit	693 km Inclination 98.18° Sun-synchronous
Repetition rate	12 days
Swath	80 Km 250 Km 400 Km
Processing levels	Level-0 Raw for SM, IW, EW modes Level-1 SLC for SM, IW, EW , WV modes Level-1 GRD for SM, IW, EW , WV modes Level-2 OCN for SM, IW, EW , WV modes Level-0 WV (not released to users)
Polarization	Single polarization (HH or VV) for SM, IW, EW , WV modes Dual polarization (HH+HV or VV+VH) for SM, IW, EW modes

a characterized by low backscattering in SAR images, which helps in flood detection. Figure 1 demonstrates the backscattering of different surfaces.

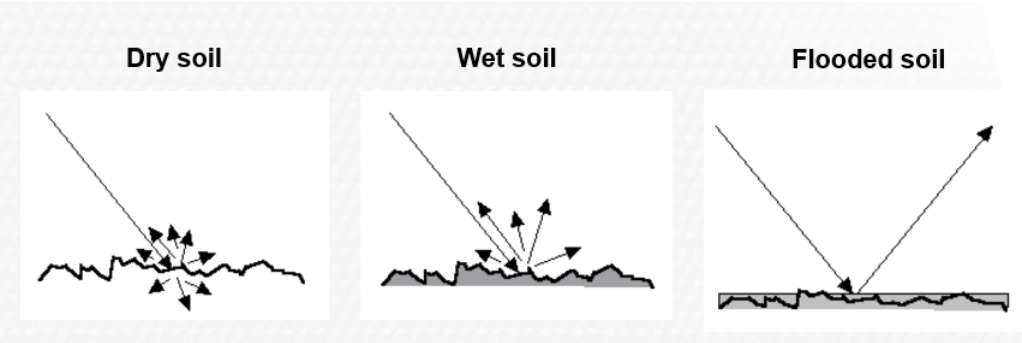

Figure 1: Backscattering of dry, wet, and flooded soils

On the other hand, areas like urban cities are affected by the double bounce effect, which results of having two smooth areas or surfaces forming a right angle facing the radar beam. Consequently, the beam bounces twice off the surfaces and the main radar

energy is reflected back to the sensor. Figure 2 illustrates the double bounce effect.

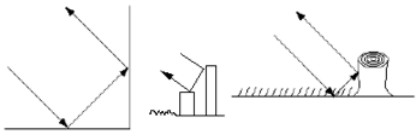

Figure 2: Double bounce effect

When obtaining data from Sentinel 1, it is important to apply radiometric calibration to the product so that the digital pixel would directly relate to the radar backscatter of the location. For level 1 products, which will be used later, the calibration is done by calculating the sigma nought and the result is backscatter coefficient (σ_0).

Beside the backscattering coefficient, interferometric techniques can be useful in flood detection for the reason that the modification of the electromagnetic characteristics of the surface possibly due to a flood cause the low coherence. When comparing coherence of region data taken before a flood event to the coherence of data of the same region after the flood, loss of coherence can appear on flood areas.

4.1.2 Optical Remote sensing

Sentinel 2 is an earth observation mission from ESA launched in June 2015, with two satellites S2A and S2B phased at 180° to each other [3]. Sentinel 2 satellites orbits are sun-synchronous, so the angle of the sun upon the surface of earth is maintained. Basic information about the satellites of the mission is shown in table 2, while table 3 gives an insight about the 13 bands captured by the satellite's Multi-Spectral Instrument (MSI) [3]. The optical sensor of the mission captures images with the behavior described in figure 3. The imaging of an object is affected by the sensor incidence angle θ, the sun elevation angle, and the height and size of the object. The optical sensor of Sentinel 2 samples 13 spectral bands as shown in table 3.

Table 2: Some of Sentinel 2 characteristics

Sentinel 2	
Resolution	10 m (4 bands) 20 m (6 bands) 60 m (3 bands
Orbit	786 km Inclination 98,1° Sun-synchronous
Repetition rate	10 days for each single SENTINEL-2 satellite 5 days at the Equator for the combined constellation
Area covered	100x100Km2
Radiometric Resolutions	12 bit by MSI
Processing levels	Level-1C and Level-2A Level-0, Level-1A and Level-1B (are not released to users)

Table 3: Sentinel 2 Bands Wavelengths

Band Number	**Band Name**	**S2A Wavelength (nm)**	**S2B Wavelength (nm)**	**Resolution (m)**
1	Coastal Aerosol	442.7	442.2	60
2	Blue	492.4	492.1	10
3	Green	559.8	559.0	10
4	Red	664.6	664.9	10
5	Vegetation Red Edge	704.1	703.8	20
6	Vegetation Red Edge	740.5	703.8	20
7	Vegetation Red Edge	782.8	779.7	20
8	Near-infrared (NIR)	832.8	832.9	10
8A	Vegetation Red Edge	864.7	864.0	20
9	Water Vapour	945.1	943.2	60
10	Short-wave Infrared (SWIR) - Cirrius	1373.5	1376.9	60
11	Short-wave Infrared (SWIR)	1613.7	1610.4	20
12	Short-wave Infrared2 (SWIR)	2202.4	2185.7	20

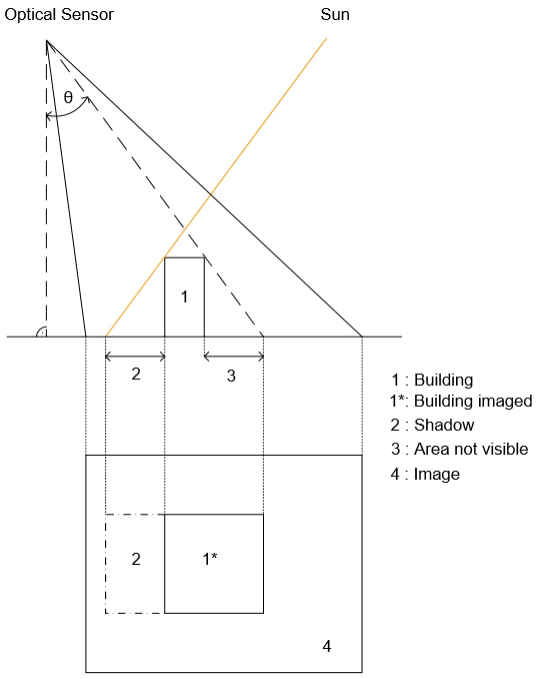

Figure 3: Imaging of a building by and optical sensor

The ability of Sentinel 2 mission to obtain data in a multitude of bands with different wavelength helps in the process of identifying inundated regions using the reflectance property of water in those bands. Thus, the optical data can be used for flood detection with water indices or automated algorithms like DNNs. The most famous indices for calculating water indices are the Normalized Difference Water Index (NDWI) and the Modified NDWI (MNDWI). NDWI is calculated using the green band and the near-infrared band, respectively bands 3 and 8, as the following

$$NDWI = \frac{(Band3 - Band8)}{(Band3 + Band8)} \tag{1}$$

NDWI is revealed to be urban land sensitive as it results in over-estimated water bodies in built-up lands. MNDWI, which is an enhanced version of NDWI, has a higher water extraction accuracy and is calculated by replacing the near-infrared band in NDWI with the short-wave infrared band, namely band 12 of Sentinel 2 data, as the

following:

$$NDWI = \frac{(Band3 - Band12)}{(Band3 + Band12)} \tag{2}$$

After the calculation of the indices, a threshold is applied to map water pixels and non-water pixels.

4.2 Deep Learning

The use of machine learning techniques, in particular deep learning, is becoming increasingly important. This tool has proven to be both powerful and efficient in multiple application fields including remote sensing. It has also been nominated as one of the ten breakthrough technologies of 2013 [13]. Deep learning uses neural networks (NN) to get high level features from raw input. The neural network is formed of multiple layers, which model nerve cells or neurons of the brain. To be called a deep neural network, a neural network should involve more than two hidden layers between the input layer and output layer.

The core unit of a neural network is the node or neuron. The earliest NNs were based on a perceptron [2], which is mathematically modeling the work of a biological brain neuron as shown in figure 4.

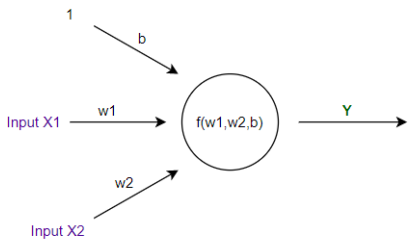

Figure 4: A single node

The node uses a function f that takes the inputs given by other nodes connected to it and calculates with a mathematical function the output to eventually transfer it to another node. The nodes are connected to each other with edges. Each edge

has a weight w, as seen in figure 4, that is used by function f to do its computation. Biases, like the bias b in figure 1, can also be added depending on the application of NN. Multiple nodes form a layer and two or more connected layers form a deep NN (DNN). In this thesis, the interest is focused on one type of neural network which is deep feedforward neural networks. These NNs do not include loops or cycles, and their layers are arranged in the following order: an input layer, two or more hidden layers, and an output layer.

The input layer nodes are given the data the user feeds to the network, and they subsequently pass it to the next layer, without performing any computations. Next, the hidden layer takes as input what is forwarded to it from the input layer and performs computations on it before forwarding it to the next layer. The performed calculations are mathematical functions, or activation functions, that introduce non-linearity into the NN. Non-linearity in the NN is crucial as it allows to model a response variable (target variable, class label, or score) that varies non-linearly with its explanatory variables, as the input of the NN is non-linear. The hidden layers are not connected with the outside world, and the output of a hidden layer is passed only to the next hidden layer or to the output layer. The final layer, or output layer, gets as input the output from the previous layer and forwards it to the user.

The task of the DNN used in this project is to classify pixel of the input image into "flood" pixel or "non-flood" pixel. Given that the model is trained with data containing image pairs and their corresponding flood masks, the learning of the DNN is supervised. The goal is to DNN is to arrive to the point of least error as soon as possible. A key concept in the learning process of the network is the calculation of the error between the predicted output of the network and the ground-truth labels, or masks in this case. The error mathematical expression is called the loss function. As stated previously, the edges have weights and biases can also be added to the activation function. Therefore, these parameters are part of the model and need to be adjusted accordingly with respect to the error of the loss function. The process of optimizing the weights and biases enables the NN to make better guesses or outputs as the parameters are adjusted according to their contribution to the overall error. The process of scoring the input, calculating the loss, and updating the parameters of the model is repeated until the error can no longer be reduced. The selection of the loss function depends on each application. For

cases where the output should have two classes, as it is the case for flood mapping with classes [flood, non-flood], one of the most used loss functions is the binary cross-entropy or log loss. Its mathematical expression is:

$$H_p(q) = -\frac{1}{N}\sum_{i=1}^{N} y_i.log(p(y_i)) + (1-y_i).log(1-p(y_i)) \tag{3}$$

where y is the label or true value and p(y) is the predicted probability of the label being flood or non-flood for all N pixels or input. Various feedforward NN architectures were introduced for various applications, like Autoencoder models, Convolutional NN models (CNN), Recurrent NN models, and Recursive NN models [3]. 4.2.1 describes CNNs. 4.2.2 and 4.2.3 describe respectively two architectures using CNNs.

4.2.1 Convolutional Neural Networks

The feedforward NN example considered in this study is a CNN. CNNs are heavily used in computer vision and image analysis applications, as they were proven to be very efficient in classification problems. They have also been used in comparing images in different contexts [19, 19, 5]. The four essential operations that define CNNs are convolution, non-linearity, and pooling [15]. Each operation will be discussed explicitly to understand how CNNs work.

Considering an image of a specific object, the goal of a CNN is to recognize or classify that object. The image of the object is represented as a matrix of pixel values, and it is taken as the input. The convolution operation enables the CNN to extract features from the input layer, which represents the image. It is done by simultaneously sliding a matrix called "filter" over the input matrix and computing the element wise multiplication. The outputs of multiplications are added up and the result is "feature map". The calculations of the convolution layer involve the calculated neuron's value by summing up all neurons' input values (x_i), the weighted inputs (w_{ij}) of the neuron plus the bias parameter (b_j), and the application of an activation function:

$$y = \sum_{i=1}^{n} w_{ij} * x_i + b_j \tag{4}$$

where * is a two-dimensional discrete convolution operator.

The activation function, or the second characteristic CNN operation, adds the non-linearity to the model because filter (convolution operation) and matrix operations are linear operations and they do not reflect the non-linearity of the raw data. The mathematical functions used as activation functions can vary depending on the application purpose, and some examples that are widely used are Sigmoid function, Tanh function, and Rectified Linear Unit function. A sigmoid function takes as input a real-valued number and maps it into a range between 0 and 1. Consequently, large negative numbers become 0 and large positive numbers become 1. The hyperbolic tangent function takes as input a real-valued number and maps it into a range between -1 and 1. Rectified Linear Unit (ReLU) function is linear for all positive values, and zero for all negative values. It is defined as:

$$f(x) = max(0, x) \tag{5}$$

Some parameters affect the size of the feature map and the main ones are the padding, the depth of filters, and the stride [8]. The padding is a parameter that helps avoid outputs shrinking and information loss on the corners of an image or feature map. When adding zero padding to the border of an input image matrix, the filter can be applied to the border elements too. The second parameter is depth, and it is the number of filters applied. Therefore, if 3 filters were applied to an image with one channel, the result would be 3 feature maps stacked as a matrix with depth of 3. The stride parameter sets how many pixels or input elements are skipped while sliding the applied filter. Thus, the future maps size decreases when the number of skipped pixels increases.

The third operation that defines CNNs is pooling. This operation enables subsampling of the output of the lower layer to reach translational invariance. The most significant information is kept while reducing the dimension of the lower layer. Applying pooling does not prevent the network from learning about slight changes in images because these changes or maxima are considered as significant since they are maxima within their respective ranges, so they are kept. It is also good to mention that pooling similarly reduces the number of computations done on the network, which regulates overfitting [14].

The CNN architecture can include at the end of it a fully connected layer used as a classifier, but it is not a characteristic operation of CNNs. Each node in the fully connected layer is connected to all nodes in the lower layer and calculate the probability of classes based on the high-level features forwarded to it by its input.

4.2.2 U-net

CNNs are also used for semantic segmentation applications. The task is achieved by assigning an object class to each individual pixel in the input image. A widely used architecture of CNNs in semantic segmentation is the U-net architecture [16]. While there are many architectures presented to do the same task, U-nets are networks that can be used when the dataset is small with excessive data augmentation techniques. Semantic segmentation with U-nets is mainly done by down-sampling of an image for feature extraction, then up-sampling using deconvolutional layers, to construct a pixel-wise classification labeled map. A deconvolution layer is simply a layer that where deconvolution operation is applied, or in other words, the transpose of a convolution operation is applied [11]. The U-net architecture consists of an encoder joined to a symmetrical decoder [11].

The encoder is a convolutional network and its task is to wrap the spatial dimension of the input image into a lot of meaningful and significant features. For this purpose, the encoder applies convolution operations followed by max pooling or down-sampling operation to encode the input image into a matrix of feature representations at different levels. The extracted features from the input image become more abstract and subsequently have more semantic information. This architecture is different from the CNN that discards all spatial information to produce high-level semantic class labels for object recognition applications. CNNs used for change detection need to preserve the spatial information to predict pixel-wise semantic changes. Thus, a decoder is essential for the change detection architecture.

The decoder is the deconvolutional network and it serves to extract these sets of features to construct a segmented or labeled representation of the input image. The decoder applies up-sampling operation, concatenation, then convolution operations. The concatenation in U-net is done by copying the features from layers in the encoder and

concatenating them with the corresponding layer (of same level) in the decoder part. This method ensures the preservation of pixels positions after convolution and max pooling operations. Consequently, U-nets can be used for change detection between two images from different time periods.

To combine what was described about the components of a U-net, figure 5 shows the structure of a U-net architecture with the main discussed operations. The input of the U-net in the figure is an image of size 256x256 with 3 channels.

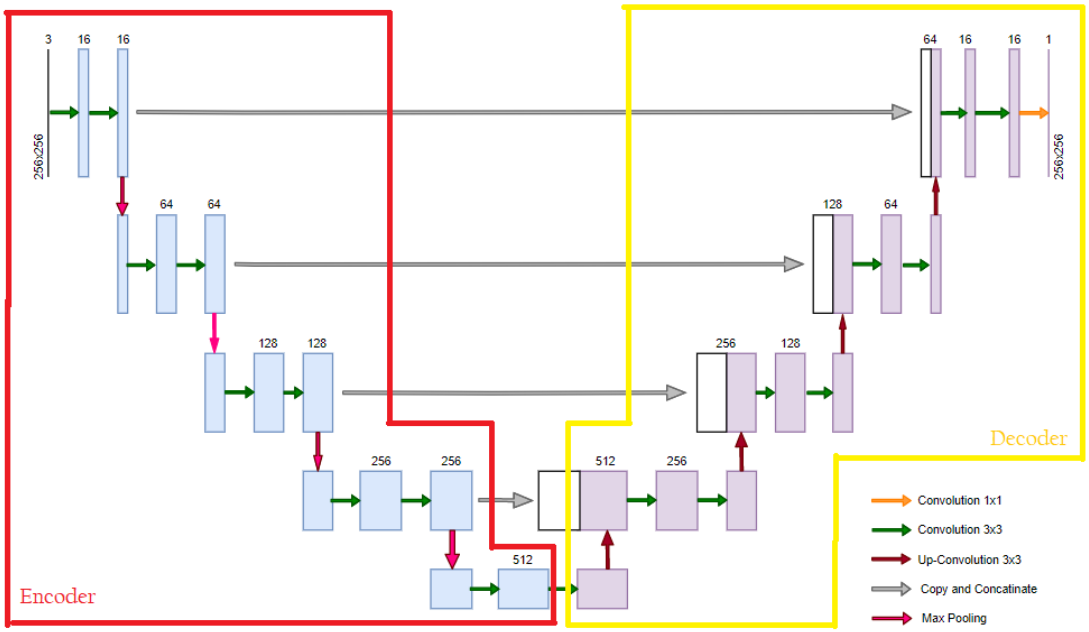

Figure 5: A U-net architecture

4.2.3 Siamese Neural Networks

Change detection is the procedure of finding the relevant changes by observing the object or area at different timeslots. Change detection is one of the main applications of remotely sensed data from satellites, for the reason that repetitive coverage is at short intervals and image quality is consistent [18]. Flood detection can be handled as a change detection problem. The specific assumption to be taken is that the detected change is related to change of water surfaces only. For this study, the semantic segmentation

is relevant since it can be adopted for change detection, and U-net is an appropriate architecture to use in this case. Because the U-net takes one input, a Siamese NN (SNN) will be used to get features from an image pair.

SNN is a network that has two branches with the same architecture and shared weights. Each branch takes one image input from the image pair, and the output of both branches is combined to give the labeled map. The choice of using SNNs is not only done for the need of feeding an image pair, but also because this methodology guarantees that feature extraction from the image pair is performed with the same approach, since both branches have the same weights and the image pairs have the same type of sensor and similar characteristics.

4.3 Flood Mapping

Although statistical or rule-based methods are widely used for detecting water and floods, there exist limitations when using these methods. The most obvious one is the selection of the appropriate threshold, as it can be a difficult task if the area covered by flood is characterized by ground variations (i.e., urban and non-urban areas). Other factors include the presence of shadows due to the illumination from the sun and atmospheric changes when using optical data. Therefore, these changes can affect the flood detection method if not taken into consideration. Selecting and preprocessing of datasets before using is necessary in this case.

As previously stated, satellite data can be very useful in case of flood events because of measurements repetition rate, the constant resolution, and its accessibility. The use of optical and SAR data is an interesting approach to compare the performance of using them in this kind of situations. They both have advantages and disadvantages so using both of them can be advantageous to compensates each other's downfalls.

SAR labeled data for floods is rarely found mainly because of its less intuitive appearance compared with optical data due to its speckle noise [10]. Therefore, the labeling task becomes more challenging to do manually. Nonetheless, it proves to be beneficial in the task of detecting water simply because the variation of the backscattering of the signal with respect to the object or surface it senses, as previously stated in Chapter 2 (Sentinel 1 section). In addition, its independence from atmospheric and sunlight

conditions can be advantages in situation of cloudy and bad weather during a flood event. The final input SAR data that will be used by the proposed algorithm consists of the coherence map of the study region and the measurements of the sigma nought values from the converted pixel values in digital numbers from two different polarizations. These 3 products will be extracted for two time periods: one before the flood event and one after the flood event.

Optical data, on the other hand, is dependent on weather conditions and cannot take measurements during nights. Consequently, the weather needs to be free of clouds to sense flood areas. If it is the case, then optical data would be easier to label manually, compared with SAR data. In addition, there is no speckle noise effect on the data. More importantly, its ability to acquire images in various wavelength bands is useful for water detection.

The satellite sensor captures RGB bands which are widely used bands in classification problems. This study focuses on using another combination of Sentinel 2 bands, which is a combination of band 3, band 8, and band 12. The motivation behind using those bands is because they are the three bands having high reflectance for pixels with clear or turbid water. Band 12 is also used because it will help to enhance the contrast between the urban land and water land, as water has a strong absorbability and great radiation in this band [20]. Figure 6 shows the reflectance of clear and turbid water with respect to the wavelengths of band 3 and band8.

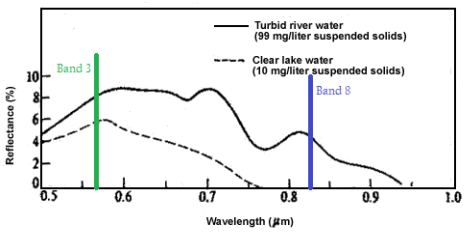

Figure 6: Reflectance of clear and turbid water with respect to the wavelengths of band 3 and band8

4.4 Conclusion

The second chapter gives a definition of concepts and some theoretical background about the knowledge needed for the description of developed approach for the thesis problematic. It also explains the motivation behind choosing to work with SAR datasets of Sentinel 1 satellite and optical datasets of Sentinel 2 satellite for flood detection using SNNs.

5 Proposed Flood Detection Model

In this chapter, the proposed model is presented. The proposed identical models to map floods are built from scratch. Hence, no pretrained models are used. All parts of the model are described in detail in sections 5.1 and 5.2.

5.1 U-net

The U-net architecture contains an encoder and a decoder. The appearance for water could be variable in different images, even if they are unchanged at semantic level. Given that semantic space is favorable to change detection, the projection to of the original image into it a good step. The U-net encoder applies this procedure. The encoder of the network consists of multiple convolution layers, max-pooling layers, and dropout layers. The outputs are semantic features from the images. The decoder takes these features to recover the spatial information and produce the flood map. Deconvolution layers, up-sampling layers, dropout layers and convolution layers are used to form the decoder.

Figure 5 shows the base U-net architecture used in this study for all flood mapping models. The input and output dimensionality is 256x256x3 in accordance with the datasets mentioned in the previous section. The hidden layers use of the ReLU activation function, and Sigmoid activation function is employed in the output layer. All convolution operations in the model have a kernel size of 3x3 and a zero padding. Each max-pooling layer and concatenation layer was followed by a dropout layer. All deconvolution operations in the model use a kernel size of 3x3, a stride of 2, and padding

of 0.

The encoder of the architecture has five levels. The first four levels have two convolution operations applied to the input image, followed by a max-pooling operation with a kernel size of 2. At the bridge, or fifth level, two convolution operations are applied, but no max-pooling operations is used. The decoder has also four levels, each consisting of one deconvolution operation, followed by two convolution operations. The final level of the decoder had a third convolution operation in order to get a one channel output as the flood map. The number of kernels at the first level of the encode is 16, and the number is doubled at each subsequent level. The number of kernels at the fifth level is 256. The opposite operation was done for the decoder. The number of filters was halved until it reached 16 again, before the final convolution was applied. The output is a flood map of size 256x256x1.

5.2 Networks

For flood mapping, an image pair is used to map the inundation by mapping water bodies from the pre flood image and subtracting it from the water bodies map of the post flood image. Therefore, the SNN introduced in the Second Chapter is used as the backbone model for flood mapping in SAR data and optical data. The overall structure is shown in figure 7, where the SNN is composed of two U-nets performing semantic segmentation on an image pair and a differentiator is used to calculate the output of the flood mapping model. It only subtract the tensors given by the two semantic segmentation networks. The structures of the U-nets are identical and both branches share the same weights due to the constraint that two images of each pair must be projected to the same semantic feature space to be compared.

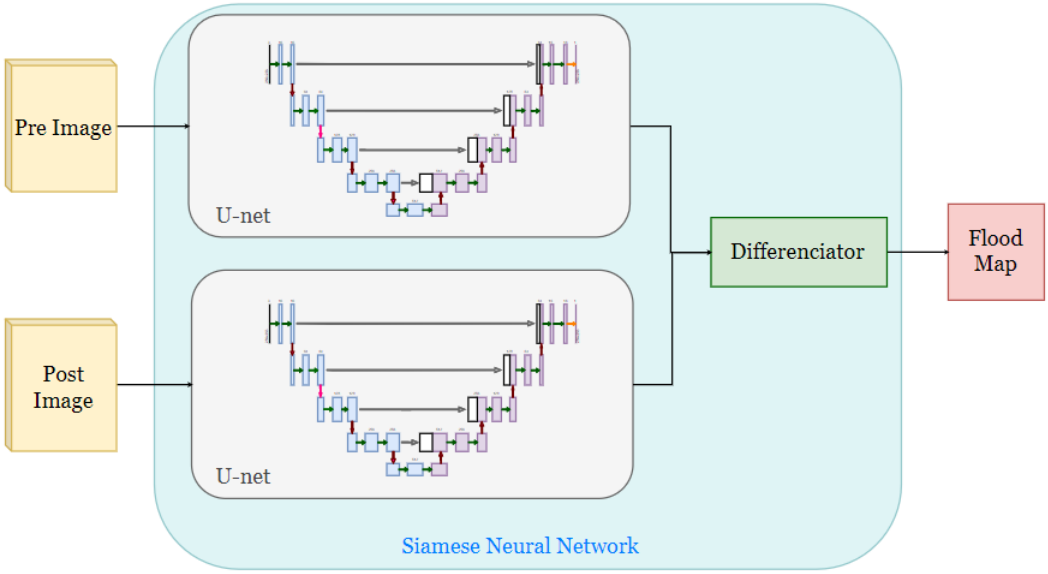

Figure 7: Overall network

6 Experimental Settings

6.1 Data Acquisition and Pre-processing

One of the major challenges with using DNNs for remote sensing applications is the availability of data. As stated earlier, labeled Sentinel 1 data is hard to find because attempts to use SAR data in deep learning only started recently. Another challenge is the faced difficulty to find Sentinel 2 data covering a flooded area without clouds.

The first considered flood events for this study were located in Europe, because some selected flood maps are made available to users through the Copernicus Emergency Management Service [1]. The service was not available for use by the public, and only authorized users were able to trigger the process of producing flood maps for the desired region. Thus, only the available flood maps accessible to the public could be checked. However, when we verified Sentinel 2 products on the corresponding dates used by the inundation mapping service for different locations, the found images were mainly covered

with clouds which prohibited the sensor from imaging the region surface. Therefore, the overall process of acquiring SAR and optical data, processing it, and producing ground truth maps was done by us.

6.1.1 Study Area

Choosing the right region for the experiment was not a task to be underestimated. The ground truth map would be mainly deduced by labeling the optical data because it is easier and practical. Hence, the sensing times of both sensors of the interest area before and after the flood should be very close to each other to assume that the ground truth is usable for both, and not only SAR data. In addition, the extent of the flood regions, the evolution of the inundation with time, and the cost of data (only free data were used) were factors that were considered.

After doing some research, two regions in Iran were selected for this study. Specifically, the region of Aq-Qala and the region of Ahwaz. The first region was inundated by the Golestan floods hitting northeast the country, which were caused by heavy rains from 19th of March 2019. This area is used for training and testing the proposed model for SAR data and the proposed model for optical data. The second region is located in southwest Iran and was hit by heavy rains too just few days after the floods in the north. It is used only for the network using optical data. Inundations in both regions were observed for longuer than 20 days. Figure 8 shows a picture of the floods taken in Khuzestan province where Ahwaz is located.

Figure 8: An aerial view of flooding in Khuzestan province, Iran, April 5, 2019

Both regions have urban and non-urban areas, and the floods submerged part of the cities, plain field, and rivers on urban and non-urban areas. Therefore, many cases were represented in the study regions.

6.1.2 Data Collection

Given the described constraints, SAR and optical data were obtained from Sentinel Scientific Data Hub [4]. Table 4 details the selected dates of satellite sensing.

Table 4: Sentinel 2 Bands Wavelengths

Satellite	**Bands Used**	**Spatial Resolution (m)**	**Date**	**Study Area**	**Data Source**
Sentinel 1 A	Dual polarized C band (VH, VV)	5x20 (SLC)	27.02.2019	Aq-Qala	[4]
Sentinel 1 A	Dual polarized C band (VH, VV)	5x20 (SLC)	11.03.2019	Aq-Qala	[4]
Sentinel 1 A	Dual polarized C band (VH, VV)	5x20 (SLC)	04.04.2019	Aq-Qala	[4]
Sentinel 2 L2A	G, NIR, SWIR2	10,20	11.03.2019	Aq-Qala	[4]
Sentinel 2 L2A	G, NIR, SWIR2	10,20	05.04.2019	Aq-Qala	[4]
Sentinel 2 L2A	G, NIR, SWIR2	10,20	22.03.2019	Ahwaz	[4]
Sentinel 2 L2A	G, NIR, SWIR2	10,20	26.04.2019	Ahwaz	[4]

For, the first region (Aq-Qala), Sentinel 2 data was obtained for two dates, one before and one after the event. The same process was done for the second region. As for Sentinel 1 data that was used only for the first region, data was for two different periods of time before the inundation and one date after the event. The reason is that the calculation of the coherence for SAR data requires two dates, so two pre event dates were used to check the coherence before the flood and two dates before and after the flood were used to calculate the coherence after the happening of the flood.

The first phase of pre-processing of the data is done in 3 main procedures: First,

optical data is transformed to 16bit georeferenced stack of bands 3, 8, and 12 by exporting the desired bands as Geotiff files in ESA SNAP tool. The data are level 2 A products, so the bands are orthophotos in UTM/WGS84 projection are radiometrically calibrated. Second, SAR data is processed in ESA SNAP tool to calculate the coherences [7] and the sigma nought values (in dB) using pixel values from digital numbers. All the final data from SAR will also be geocoded. Finally, optical and SAR data are used to produce a flood map as the ground truth using statistical methods and manual labeling in QGIS and ENVI software products.

Figure 9 shows the stack of the NIR, Green, and SWIR bands (displayed respectively in RGB) for data before and after the flood in Aq-Qala region. Figure 10 shows similarly the stack of bands for Ahwaz.

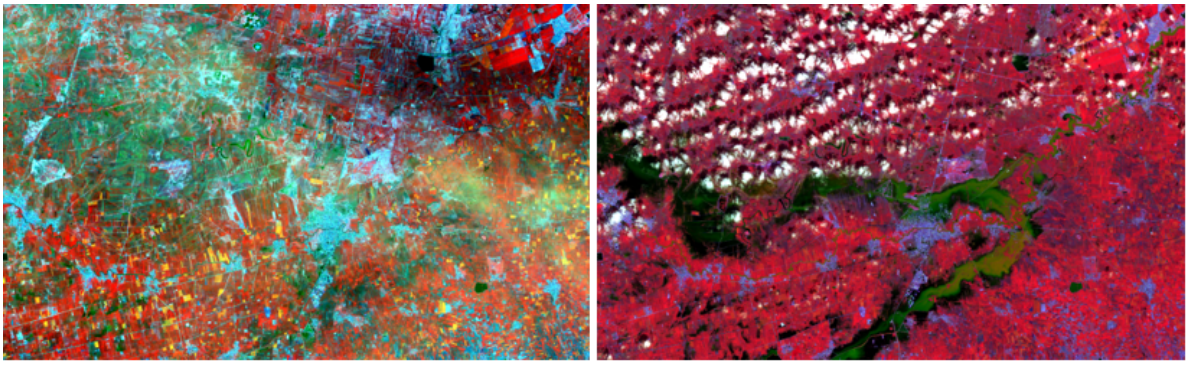

Figure 9: Aq-Qala optical data. (Left: R, NIR, SWIR composite of 11.03.2019. Right: R, NIR, SWIR composite of 05.04.2019)

Figure 10: Ahwaz optical data. (Left: R, NIR, SWIR composite of 22.03.2019. Right: R, NIR, SWIR composite of 26.04.2019)

The Calculation of the coherence is the first step that is part of SAR data preprocessing, as it will be one of the three channels fed to the model for change detection. It's computation data is done in the following steps in order using SNAP tool:

- Data from two different time stamps are coregistred in the software. It is possible to do this operation with only one swath from each input. After checking the data from Sentinel 1 and Sentinel 2, sub-swath 1 was chosen as it covers the intersection area between all products. Therefore, only one part of the data is clipped and used for further processing.
- The Coherence is calculated from the coregistred data files.
- The data acquired with IW mode is tiled as swaths and bursts. So coherence is debursted to link all the bursts into one image.
- Speckle noise is reduced from the coherence using Lee filter

- Terrain Correction is applied to the output without noise
- The output is exported as a one band Geotiff image

The mentioned steps above are for the data of 11th of March and 27th of February to get the coherence before the flood event and it is similarly done for the data of 11 of March and 4th of April to get the coherence after the flood event. As seen in table hh, SAR data is obtained with two polarizations. Thus, two intensities will be calculated for both the 11 of March (pre flood) and the 4th of April (post flood). The process of calculating one intensity is using the following steps in order:

- The data is clipped to the area used in the first the step of the coherence computation for both dates.
- The output of the first step is used to calculate the sigma nought value σ_0 of the pixels to apply radiometric calibration.
- The output from the second step is debursted to link all bursts into one image
- Speckle noise is reduced using Lee Filter
- Terrain correction is applied to the output without noise
- The output is exported as a one band Geotiff image

Hence, the processes for computing the coherences and intensities of SAR data result in 6 one-band images: 2 coherence images for before and after the flood and 4 intensities in VH and VV polarisations for pre and post flood. The final image pairs used by our proposed model will be stacked as [coherence, intensity VH, intensity VV].

Figure 11 shows the resulting SAR images that will be used later in our algorithm. The flood area can be visually seen when comparing both images.

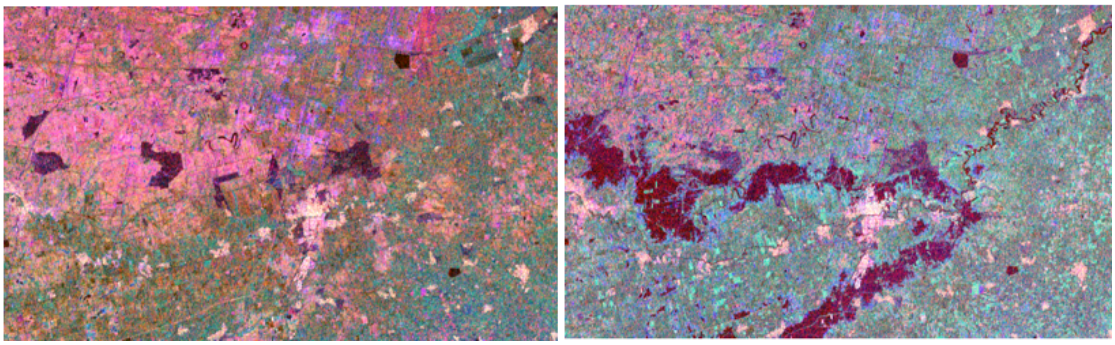

Figure 11: Aq-Qala SAR data. (Left: coherence, intensity VH, intensity VV composite of 11.03.2019. Right: coherence, intensity VH, intensity VV composite of 04.04.2019)

The products from all sensors need to be georeferenced. When imported to QGIS software, all optical and SAR images are projected to the same coordinates system. The intersection of all images ends with all images being clipped to the following rectangle with the coordinates in EPSG:32640 - WGS 84 / UTM zone 40N:

- x-axis bound: [252060.00 , 290570.00]
- y-axis bound: [4090610.00 , 4113890.00]

For the optical data used only by the algorithm for optical data flood detection, its bounding box is has the following coordinates projected in EPSG:32639 - WGS 84 / UTM zone 39N:

- x-axis bound: [206640.00 , 296930.00]
- y-axis bound: [3391990.00, 3491160.00]

6.1.3 Data Labeling

[12] evaluation of NDWI and MDWI for the assessment of waterlogging concluded that MNDWI showed a high accuracy in achieving the task since it scored positive values for water features mixed with vegetation and in flooded build up features. Therefore, MNDWI can be used as part of the process of labeling the floods in the study area to

get the flood map. Also, from figure 11, the flood shape can be visualized in the SAR data with dark pixels, thus it will be used too to produce the ground truth map. Using SNAP and Matlab, MNDWI is computed and after apply a threshold of 0,67 on the index, a first version of the flood mask is obtained. Some parts of the flood in the city of Aq-Qala cound not be included using this threshold, therefore ENVI software was used to manually labels those areas using optical bands and SAR bands visualizations. The final flood map is displayed in figure 12.

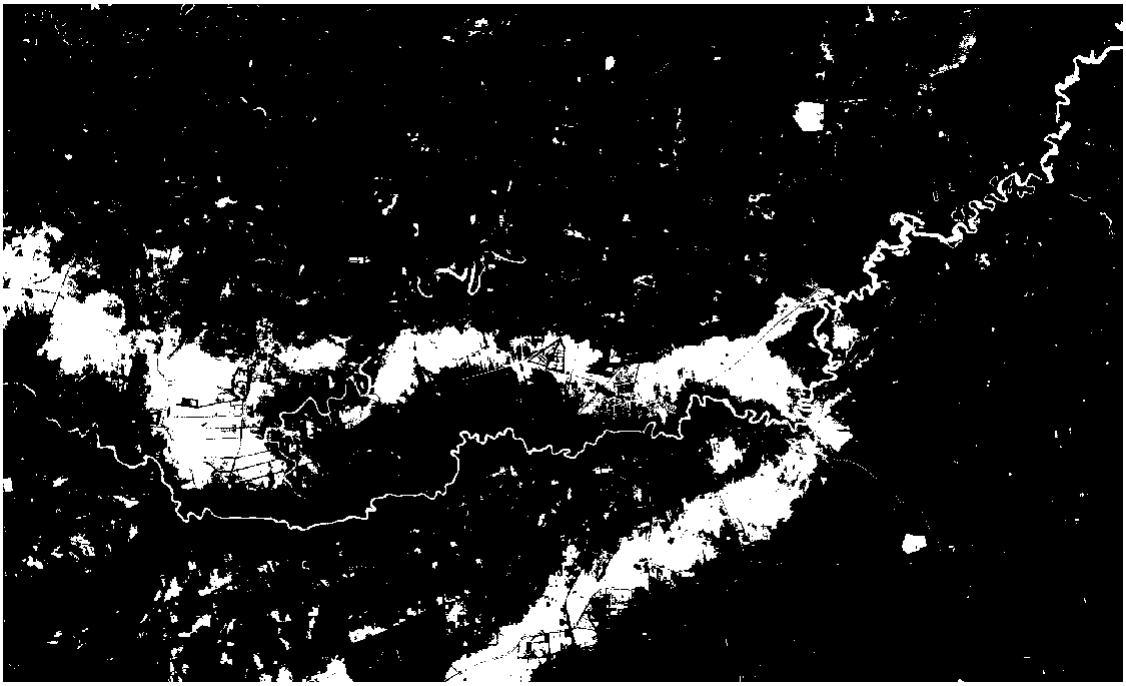

Figure 12: Final flood mask of Aq-Qala region

The same process was applied for the data of Ahwaz region. Because there was no SAR data for this region, a ground truth map was obtained later from Copernicus that gave flood maps for some intersection regions after checking its accuracy using flood area maps produced by official authorities. The two maps were compared and the label map obtained is shown in figure 13.

Figure 13: Final flood mask of Ahwaz region

6.1.4 Data Normalization

Minmax normalization was performed on geo-referenced images before feeding them to the network. Normalization is an essential step required in the field of data mining, because it helps to scale the values to fall within same specific ranges and may contribute to enhancing the accuracy of the machine learning. In this study, normalization helps to remove different ranges of spectral reflectance values present in images.

6.1.5 Data Augmentation

It is important to note that data augmentation is done while considering the balancing of data labels. In other words, the final optical and SAR datasets should have balanced flood and non-flood pixels numbers balanced. First, after computing the number of labels in each class, the results show that non-flood pixels are outnumbering flood pixel by a big number. Therefore, after tiling the images into 256 by 256 with 3 channels, the patches having a large flood area are augmented until the classes are more or less balanced. Finally, the data is shuffled and split into training, validation and testing sets with the percentages 64%, 16%, 20% respectively.

6.2 Network Structure implementation

Tensorflow is a widely used open-source platform that simplify the implementation of machine learning algorithms. Keras is an API on top of Tensorflow that helps building and training DNNs. The proposed model is implemented using these open-source libraries. The model runs on a GeForce GTX 1060 GPU server with 3GB.

6.3 Evaluation Metrics

The confusion matrix is the evaluation measure used for assessing flood detection performance. Table 5 shows the confusion matrix used in this experiment.

Table 5: The confusion matrix

confusion matrix		**Predictions**	
		Flood	**Non-flood**
Truth	**Flood**	True Positive (TP)	False Negative (FN)
	Non-flood	True Positive (TP)	False Negative (FN)

The matrix has four simple criteria based on it that measure how the predicted values are close to the true values:

- The accuracy A that calculates the accuracy of correctly labeled pixels in the total

number of pixels. Its mathematical expression is:

$$A = \frac{(TP + TN)}{(TP + TN + FP + FN)} \tag{6}$$

- The recall R that determines how many flood pixel are correctly classified. Its mathematical expression is:

$$A = \frac{TP}{(TP + FN)} \tag{7}$$

- The precision calculates the fraction of pixels correctly labeled as flood pixel. Its mathematical expression is:

$$A = \frac{TP}{(TP + FP)} \tag{8}$$

- F1 score measures the balance between the criteria R and P. Its mathematical expression is:

$$A = \frac{2 * R * P}{(R + P)} \tag{9}$$

Pixel accuracy is an evaluation method where the percent of pixels in the image which were correctly predicted is calculated. This metric can sometimes provide misleading results when there is no balance in class representations on the dataset, because the method is mainly reporting how well the class with the highest representation is predicted. Given that class balance was verified in both datasets, this evaluation criteria can be used for evaluation.

7 Experimental Results

This section discusses the methodology used to conduct the study. Section IV-A lists the training algorithm parameters, and Section IV-B presents the performance of both models.

7.1 Training Algorithm Parameters

To train and test the networks, tensorflow platform is used. The input data images have a common size which is 256x256x3. For the model based on optical data, a total of 1820 pairs of images were used. These pairs include data from the first region and the second region of study. The data was split into training, validation and testing sets with the percentages 64%, 16%, 20% respectively. As for the model based on SAR data, only 304 pairs of images were used as SAR data was available for the first area of study only. The splitting of data into training, validation and testing sets was done in the same way as it was done for the optical data.

The model parameters are initialized with a normal distribution centered at 0. The optimization of the parameters is done by using the binary cross-entropy function to compare the predicted values with the ground truth. The parameters are then optimized using Adam technique [9]. The learning rate is initially set to 0.00001 and it is reduced by a factor of 0,1 when the validation accuracy is not increasing after 3 epochs. The SNN for flood mapping using optical data was trained for 33 epochs and figure 14 shows the accuracy and loss results for the training phase.

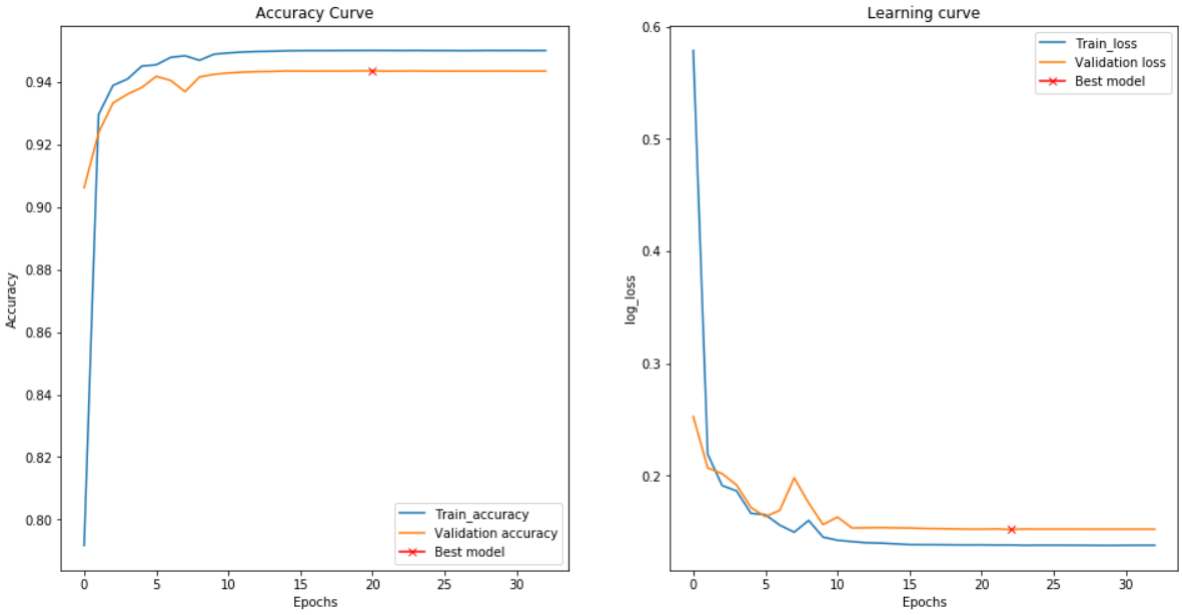

Figure 14: Optical data based network training and validating accuracies and losses (learning) curves

The SNN for flood mapping using SAR data was trained for 40 epochs and figure 15 shows the accuracy and loss results for the training phase.

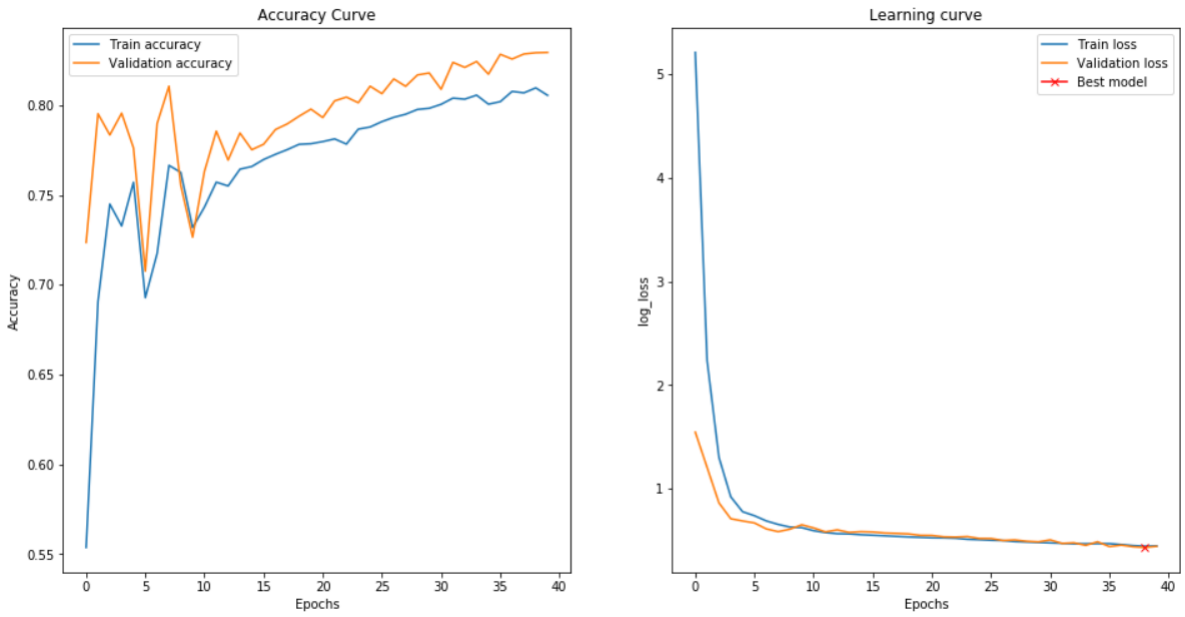

Figure 15: SAR data based network training and validating accuracies and losses (learning) curves

For both networks, the best model was chosen with consideration to the lowest validation loss value.

7.2 Flood Mapping Results

Table 6 summarizes the performance of the 2 models based on the evaluation metrics.

Table 6: Evaluation results

	SNN for flood detection in SAR data	**SNN for flood detection in SAR data**
Accuracy	95.02%	80.43%
Accuracy of flood class	85.02%	73.66%
Accuracy of non-flood class	95.26%	82.24%
Recall	95.02%	80.43%
Precision	95.90%	84.04%
F1 score	94.67%	81.00%

The flood detection using optical data performed quite well according to the evaluation factors. The detection of non-flood areas did better that the detection of flood areas, but considering the small amount of training data, the results can be considered as acceptable. Figures 16 - 19 show some results of flood maps. On each figure, the left plot is the NIR (second channel) of the pre-flood image, the second-to-left plot is the second channel of the post-flood image, the central plot is the ground truth map, the fourth plot is the flood prediction map before applying the threshold and the last plot (right plot) is the final predicted flood map using the threshold. On all plots, the borders of the flood areas are included to facilitate the visualization of the flood area.

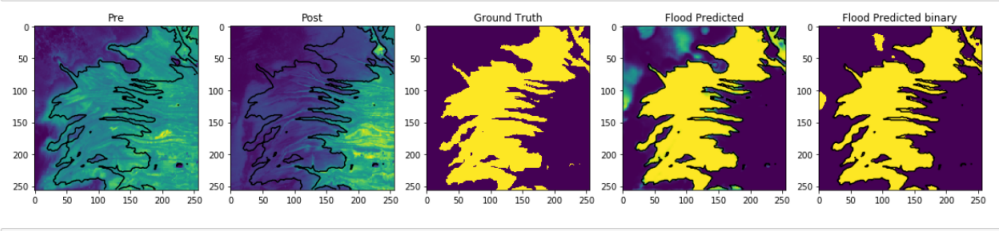

Figure 16: Flood detection results.

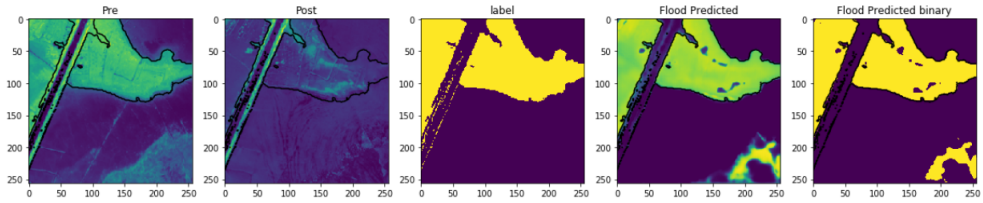

Figure 17: Flood detection results

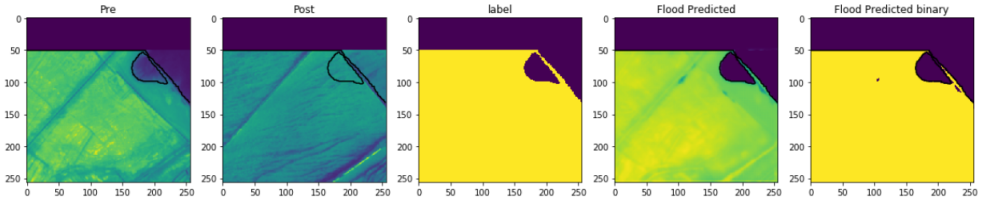

Figure 18: Flood detection results

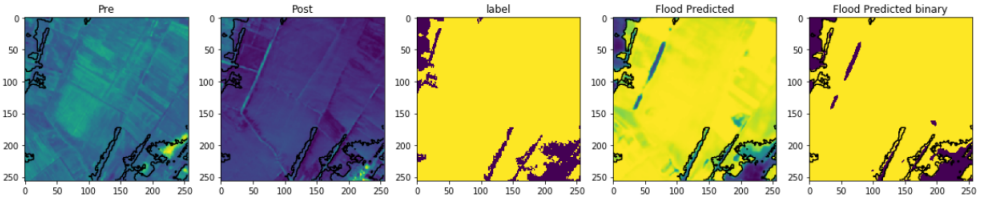

Figure 19: Flood detection results

As for SAR based flood detection model, the results were not better. The model also performed better at predicting non-flood pixels, but given the small amount of data, the model performed better than expected. Figures 20 - 22 show some results of flood maps. On each figure, the left plot is the pre-flood image, the second-to-left plot is the post-flood image, the central plot is the ground truth map, the fourth plot is the flood prediction map before applying the threshold and the last plot (right plot) is the final predicted flood map using the threshold. On all plots, the borders of the flood areas are included to facilitate the visualization of the flood area.

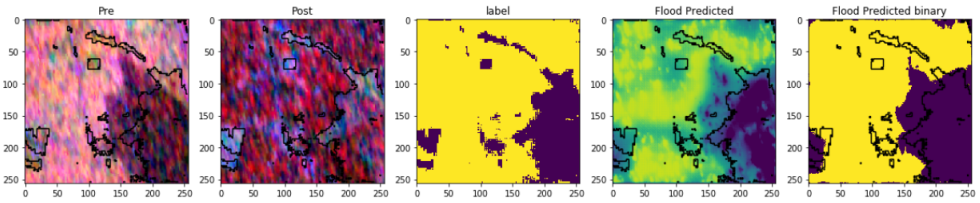

Figure 20: Flood detection results

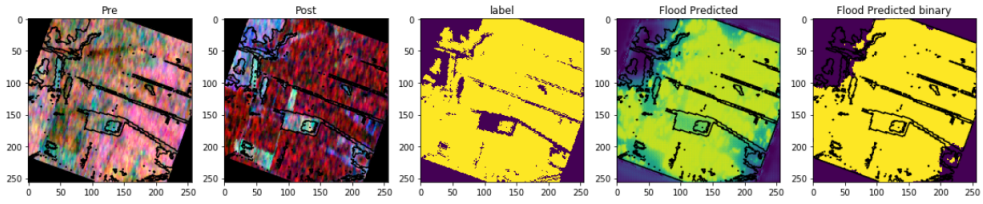

Figure 21: Flood detection results

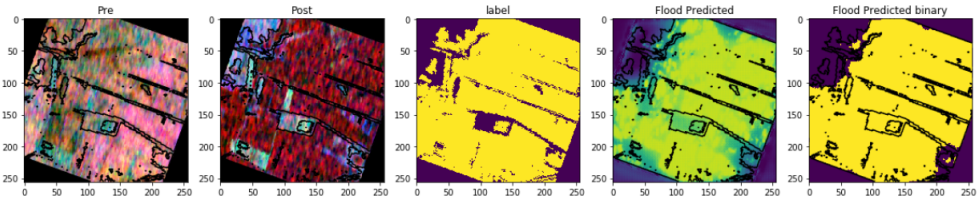

Figure 22: Flood detection results

7.3 Discussion

The process of comparing flood detection models using different remote sensing data is complex task because it requires an understanding of the complicated relationships between the flood and the satellite characteristics. Throughout this experiment, the following factors are considered to be key parameters in this task:

- Weather conditions are important as they influence the results of optical data. Clouds did affect optical data availability in the northwest of Aq-Qala region. SAR was used to check cloudy areas in Aq-Qala, but these regions were not affected by floods.
- Noise of SAR data is another factor that affected the performance of flood mapping.

The deep learning approach performance can be considered as efficient in terms of time, cost, and performance. When satellite optical data data is available during and after floods, this methodology can quite useful in supplying quick results of flood mapping in emergency situations. Nonetheless, there is much space for improvements to be done to achieve better results. The original datasets for both optical and SAR images were heavily unbalanced, as the non-flooded area was the biggest in both study areas used in the experiment. Because of the balancing of classes constraint, many images minimum flood to non-flooded areas were not included in the training, validation, or testing of the algorithms. Therefore, the datasets used were not enough to give better accuracy results.

Given that U-nets proved to be efficient to use for cases where data is not abundantly

available, future work include training a single U-net only for sematic segmentation of individual images, and then use this trained network in a Siamese network to do flood detection for other similar datasets.

8 Conclusion

This thesis presented two models for flood detection. The first model is using optical satellite data from Sentinel 2 and the second model uses SAR satellite data from Sentinel 1. We showed how a Siamese network was able to learn segmentation of SAR and optical satellite data from the proposed methods. The accuracy of the first model for detecting flood pixels in images reached 81% and a 94,67% percent of f1 score, which can be assumed as very satisfying results given the small number of data the network trained on and the various cases of water reflectance included in the dataset. The second model accuracy in The purpose was to make costless and fast algorithms for flood detection using different satellite sensor modalities. Future work include the use of other satellites to compare results with Sentinel 1 and Sentinel 2 data. Also, a network that combines both optical and SAR data would be interesting to check its effectiveness compared to a uni-sensor modal network. Additional efforts can be made to eliminates the task of choosing a threshold after differentiating the segmentation maps of the Siamese sub-networks.

References

[1] Copernicus emergency management service (© 2019 european union), emsr352-floods in iran.

[2] Sentinel- 1.

[3] Sentinel- 2.

[4] Sentinel scientific data hub.

[5] S. Chopra, R. Hadsell, and Y. Lecun. Learning a similarity metric discriminatively, with application to face verification. *2005 IEEE Computer Society Conference on Computer Vision and Pattern Recognition (CVPR05)*, page 539–546.

[6] Yun Du, Yihang Zhang, Feng Ling, Qunming Wang, Wenbo Li, and Xiaodong Li. Water bodies' mapping from sentinel-2 imagery with modified normalized difference water index at 10-m spatial resolution produced by sharpening the swir band. *Remote Sensing*, 8(4):1–19, 2016.

[7] Giorgio Franceschetti and Riccardo Lanari. *Synthetic aperture radar processing*. CRC Press, 1999.

[8] Li F. Johnson J Karpathy, A. Convolutional neural networks for visual recognition. stanford computer science lecture.

[9] Diederik Kingma and Jimmy Ba. Adam: A method for stochastic optimization. *International Conference on Learning Representations*, 12 2014.

[10] E.e. Kuruoglu and J. Zerubia. Modeling sar images with a generalization of the rayleigh distribution. *IEEE Transactions on Image Processing*, 13(4):527–533, 2004.

[11] Hyeonwoo Noh, Seunghoon Hong, and Bohyung Han. Learning deconvolution network for semantic segmentation. *2015 IEEE International Conference on Computer Vision (ICCV)*, page 1520–1528, 2015.

[12] Igor Ogashawara, Marcelo Curtarelli, and Celso Ferreira. The use of optical remote sensing for mapping flooded areas. *International Journal of Engineering Research and Application*, 3:1956–1960, 10 2013.

[13] Person. 10 breakthrough technologies 2013, Dec 2015.

[14] Filip Radenovic, Giorgos Tolias, and Ondrej Chum. Fine-tuning cnn image retrieval with no human annotation. *IEEE Transactions on Pattern Analysis and Machine Intelligence*, 41(7):1655–1668, Jan 2019.

[15] Waseem Rawat and Zenghui Wang. Deep convolutional neural networks for image classification: A comprehensive review. *Neural Computation*, 29(9):2352–2449, 2017.

[16] Olaf Ronneberger, Philipp Fischer, and Thomas Brox. U-net: Convolutional networks for biomedical image segmentation. *Lecture Notes in Computer Science Medical Image Computing and Computer-Assisted Intervention – MICCAI 2015*, page 234–241, 2015.

[17] Sashikant Sahoo, Raj Setia, Shashikanta Sahoo, Avinash Prasad, and Brijendra Pateriya. Evaluation of ndwi and mndwi for assessment of waterlogging by integrating digital elevation model and groundwater level. *Geocarto International*, 30, 07 2015.

[18] Ashbindu Singh. Review article digital change detection techniques using remotely-sensed data. *International Journal of Remote Sensing*, 10(6):989–1003, 1989.

[19] Simon Stent, Riccardo Gherardi, Björn Stenger, and Roberto Cipolla. Detecting change for multi-view, long-term surface inspection. *Procedings of the British Machine Vision Conference 2015*, page 127–1, 2015.

[20] Hanqiu Xu. Modification of normalised difference water index (ndwi) to enhance open water features in remotely sensed imagery. *International Journal of Remote Sensing*, 27(14):3025–3033, 2006.